Electrothermally-Aware Multi-objective Modular Design: A Case Study on Series-Parallel Hybrid Propulsion Systems

Kailong Liu
Warwick Manufacturing Group
University of Warwick
Coventry, U.K.

Ji Li*
Department of Mechanical Engineering
University of Birmingham
Birmingham, U.K.
j.li.1@bham.ac.uk

Chong Zhu
School of Mechanical Engineering
Shanghai Jiao Tong University
Shanghai, China

Tao Chen
School of Electrical Engineering
Southeast University
Nanjing, Jiangsu, China

Kang Li
School of Electronic and Electric Engineering
University of Leeds
Leeds, UK

Quan Zhou, Hongming Xu
Department of Mechanical Engineering
University of Birmingham
Birmingham, U.K.

Abstract—**This paper introduces an effective modular design solution for series-parallel hybrid propulsion systems (HPSs) based on a battery electrothermal model and a sub-objective related to temperature to concurrently consider both the battery electrical and thermal behaviors. To ensure that more optimal design options are provided, a Pareto-augmented collaborative optimization (PACO) framework is proposed to integrate three multi-objective evolutionary algorithms (MOEAs), aiming to extend the range of the Pareto frontier. Furthermore, two real driving cycles taken from worldwide harmonized light vehicles are utilized to evaluate the performance of the optimized vehicle systems. The modelling results show that the decomposed MOEA (MOEA/D) within PACO is the main contributor to the performance improvement in the modular design of HPSs, which leads to the reduction of intergenerational distance by over 2.7% and increase of the hypervolume by over 17.6%, in comparison with two state-of-the-art evolutionary algorithms.**

Keywords—Battery electrothermal dynamics; multi-objective evolutionary algorithm; modular design; plug-in hybrid electric vehicle.

I. INTRODUCTION

Rising concerns on the air pollution related to transportation and air pollution is driving the vehicle industries to explore alternative low-carbon solutions [1]. To achieve this, hybrid prolusion systems (HPSs) are widely utilized as an effective way to mitigate the increasing air quality issues of the off-gas emission from conventional internal-combustion-engine (ICE) vehicles [2]. In comparison with pure electric vehicles, HPSs generally are driven over long distances and control emissions more flexibly such as at the green district in a city, or to run at a high-power mode when the emissions are of less concerns.

The speedy development of informatics provides a quicker and effective way for intelligent vehicle modular design. In this research field, heuristic algorithms are usually adopted to handle NP-complete issues. Recently, University of Birmingham proposed the improved evolutionary algorithm with chaos attractive policy for the energy management scheme design for on-road vehicles [3,4] and off-road vehicles [5]. However, these single-objective optical solutions are proven to be hard to build a Pareto frontier with good distribution, particularly for two or more objectives which need to be considered.

As one of the primary energy storage sources in HPSs, battery may exhibit different thermal and electrical operated dynamics [6]. Due to the merits such as the computational efficiency, equivalent circuit model (ECM) [7-9] has been extensively utilized to obtain real-time battery electrical behavior. Regarding the battery thermal performance, by the assumption of the evenly distributed heat generation within a battery, a thermal model with two stages has widely used to describe both the internal thermal dynamics and battery surface [10-12]. Some coupled electrothermal models have achieved the huge developments to reflect the strongly-coupled relations between battery thermoelectricity dynamics [13]. In addition, the lumped electrothermal models [14] with a streamlined order and relatively fewer model parameters are applied widely and practically. Even so, due to the heavily increased system complexity, battery thermal dynamic would be regularly unnoticed in the HPSs' system-level modular design.

In order to consider both battery thermoelectricity dynamics in the modular design of HPSs, an optimized modular design solution based on an efficient battery electrothermal model, and a sub-objective related to temperature is proposed in this study. Specifically, through coupling a RC sub-model with second order and an additional thermal sub-model with two statuses, the electrothermal model could efficiently obtain the thermoelectricity dynamics of battery. For providing customer

the further optimized allocation countermeasures, a Pareto-augmented collaborative optimization (PACO) framework is derived through integrating three multi-objective evolutionary algorithms (MOEAs). In this context, this system is capable of absorbing their merits in handle such multi-objective issue for constructing a more realistic approximated Pareto frontier to provide more design options.

The remaining parts of this paper is followed as: Section II introduces the powertrain and scalable modules. Section III formulates the optimization problem. Section IV describes the enhanced modular design solution considering the electrothermal dynamics. Detailed experimental studies utilizing the driving cycle as well as the results of 1) many-objective optimization; and 2) the robustness of vehicle system is discussed in Section V. Section VI summarizes the conclusions.

II. POWERTRAIN AND RELATED MODULES

The HPS in this study consists of an internal combustion engine (ICE), an integrated starter generator (ISG), and a trans-motor such as the electric motor with float stator [15]. According to Fig. 1, the speeds of both the ICE and trans-motor could be decoupled based on the topology of this powertrain configuration, hence these speeds could be selected freely. Here the vehicle data sourced from the ADVISOR software is used for the analysis and design of this powertrain system.
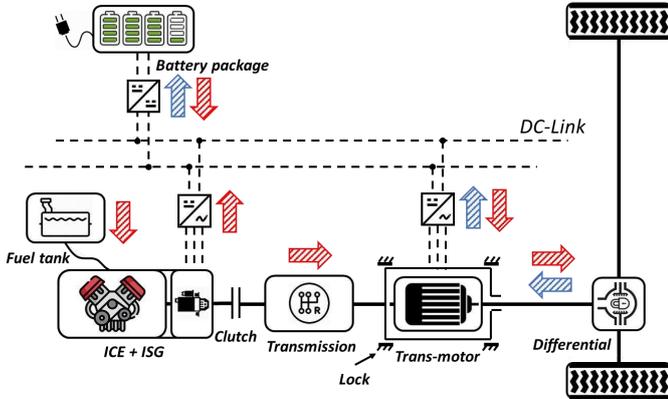
Fig. 1. The structure of the studied HPS

To be specific, a backward-facing vehicle model which takes the vertical dynamics into account is adopted. Here the demands of torque τ_d and rotation speed n_d based on the bi-level gear speed reducer are:

$$\left.\begin{array}{c}\tau_d = \left(\delta ma + \dfrac{C_d A_f u^2}{21.15} + mg\sin\theta + mgf\cos\theta\right) \cdot \dfrac{R_{wh}}{i_0 \cdot \eta_{i0}} \\ n_d = 9.55 \cdot \dfrac{u}{3.6 \cdot R_{wh}}\end{array}\right\} \quad (1)$$

where, $g = 9.81 m/s^2$ represents the gravitational constant; $\delta = 1$ and $f = 0.015$ stand for the equivalent mass inertia and rolling friction coefficient, respectively; u represents the vehicle speed with the unit of km/h; 21.15 is the transformation coefficient under the windless environment; $\theta = 0$ stands for the slope level; 9.55 and 3.6 are two

conversion coefficients from curvature per second to rotation per minute, and from meter per second to kilometer per hour, respectively. For validation purpose, the HPS is assumed to have an offered energy budget which focuses on a particular journey.

A. Internal-Combustion-Engine Module

In this study, an experimental ICE model based on a 1.9 L Saturn spark ignition engine [16] is adopted to design the module. Using Willans approximation method [17], the engine's maximum power could be scaled based on the consideration of its movement, and the equivalence power of fuel consumption could be scaled based on the engine movement as:

$$P_{f,L_{ice}} = \frac{L_{ice}}{L^*} \cdot H_f \cdot \dot{m}_f(T_{ice}, n_{ice}) \quad (2)$$

where L_{ice} and L^* are the candidate engine displacement and baseline engine displacement in liters, respectively; $\dot{m}_f$ and H_f are the instantaneous fuel consumption in g/s, and heat value for gasoline oil (46×10^6 J/kg), respectively.

B. Li-ion Battery Electrothermal Coupled Module

For effectively capturing thermoelectricity dynamics of batteries, a state-of-the-art coupled electrothermal model is built, which consists of a RC sub-model with second order and a concentrated thermal sub-model. For this coupled battery model, both the state-of-charge (SoC) $SoC(t)$ and RC voltages $(V_1(t), V_2(t))$ of battery versus time t can be represented by (3a) to (3c) separately, whilst the surface as well as internal core temperatures $T_s(t)$ and $T_c(t)$ versus t can be formulated by (3d) and (3e), respectively.

$$\frac{dSoC(t)}{dt} = \frac{I(t)}{C_n} \quad (3a)$$

$$\frac{dV_1(t)}{dt} = \frac{V_1(t)}{R_1(t)C_1(t)} + \frac{I(t)}{C_1(t)} \quad (3b)$$

$$\frac{dV_2(t)}{dt} = \frac{V_2(t)}{R_2(t)C_2(t)} + \frac{I(t)}{C_2(t)} \quad (3c)$$

$$\frac{dT_s(t)}{dt} = \frac{T_{amb} - T_s(t)}{R_u C_s} - \frac{T_s(t) - T_c(t)}{R_c C_s} \quad (3d)$$

$$\frac{dT_c(t)}{dt} = \frac{T_s(t) - T_c(t)}{R_c C_c} + \frac{Q(t)}{C_c} \quad (3e)$$

where $I(t)$, $R_1(t)C_1(t)$, $R_2(t)C_2(t)$ represent the existing parameters of first RC pair and second RC pair versus t, separately. C_n and T_{amb} represent battery nominal capacity and ambient temperature, respectively. R_u, R_c, C_s, C_c reflect the parameters of thermal sub model. Here the heat generation $Q(t)$ in (3e) can be calculated as:

$$Q(t) = I(t)T_c(t)\frac{dOCV(t)}{dT_c(t)} + I(t)\big(V(t) - OCV(t)\big) \quad (4)$$

It should be known that open circuit voltage (OCV) usually displays a nonlinear relationship related to battery SoC, while the battery terminal voltage $V(t)$ is described as:

$$V(t) = OCV\big(SoC(t)\big) + R_0(t)I(t) + V_1(t) + V_2(t) \quad (5)$$

This battery coupled model has been well-validated for A123 26650 battery, while its exact parameter values can be found in [18].

C. Energy Management Module

In this study, a typical state machine [20] is adopted in the energy management module to control the transition among three operation modes. Here three input parameters: vehicle torque requirement, T_d, speed requirement, n_d, and battery charge status, SoC is input parameter of the state machine controller, while the output is a split power vector defined as:

$$\xi = [T_{mot} \quad n_{mot} \quad T_{ice} \quad n_{ice} \quad P_{gen}] \quad (6)$$

where T_{mot} and n_{mot} represent trans-motor torque requirement and speed requirement, separately, while P_{gen} stands for the ISG power demand.

For the EV mode ($SoC > 0.5$ or $P_d < 0$), HPS would be operated like a battery-based EV, leading the split power vector under EV mode becomes:

$$\xi = [\tau_d \quad n_d \quad 0 \quad 0 \quad 0] \quad (7)$$

For the series and parallel modes ($SoC \leq 0.5$ and $P_d \geq 0$), power demand P_d with the control parameter ϕ_{mode} decides the switching series and parallel modes. Here the vehicle runs parallel mode when $P_d > \phi_{mode}$. Besides, the vehicle will run the series mode. The power-flow vector of the series mode becomes:

$$\xi = [\tau_d \quad n_d \quad \tau'_{ice}(P_{gen}) \quad n'_{ice}(P_{gen}) \quad P_{gen}^+ \cdot \chi_2] \quad (8)$$

The power-flow vector for parallel mode is:

$$\xi = [\tau_d \quad n_d \cdot (1-\chi_1) \quad T_d \quad n_d \cdot \chi_1 \quad 0] \quad (9)$$

where, τ'_{ice} and n'_{ice} are ICE's optimal torque and speed, respectively. P_{gen}^+ reflects the ISG's maximum power; χ_i (i=1 or 2) is a SoC-dependent factor mentioned below, while χ_1 and χ_2 represent the control of ICE and ISG, respectively [2].

$$\chi_i(SoC) =$$
$$= \begin{cases} 1, \; SoC \in [0,0.2] \\ \left\{1 + \exp\left[\left(\frac{SoC}{SoC^*} + \phi_{i,\beta}\right)\phi_{i,\alpha}\right]\right\}^{-1}, SoC \in (0.2,0.5] \\ 0, \; SoC \in (0.5,1] \end{cases} \quad (10)$$

where, SoC^* is a scaling factor for the SoC of the battery to improve the searching efficiency for parameters $\phi_{i,\beta}$ and $\phi_{i,\alpha}$. Here $\phi_{i,\alpha}$ (i=1 or 2) $\in [0.01,50]$ and $\phi_{i,\beta}$ (i=1 or 2) $\in [-6,6]$ are the control parameters for allowing the cut-in timing and transformation speed optimization of both ICE and ISG, while both the curve and position in this logistical function are defined separately.

III. Problem Formulation

Three optimization objectives are considered in this study: 1) the consumption of fuel from both fuel storage as well as electricity storage; 2) sum cost of both ICE and battery modular; and 3) the integral-squared-error (ISE) of batteries' mean and ambient temperature. Detailed description of each objective is shown as follows. The first objective is derived by considering the energy-saving efficiency as:

$$J_1 = \int_0^t \left(P_{f,L_{ice}} + \text{Num}_{bc} \cdot V_{oc}(SoC) \cdot I_{bc}\right)dt \quad (11)$$

where, $P_{f,L_{ice}}$ means the equivalence power of the sum consumption; Num_{bc} means the count of battery cells; V_{oc} and I_{bc} are open circuit voltage and current, respectively. The sum cost of both ICE and battery modular as the second objective

could directly affect the acceptance of customers and be described by:

$$J_2 = 12P_{ice}^{max}(C_{ice}) + 424 + C_{cell} \cdot \text{Num}_{bc} \quad (12)$$

where, C_{ice} is the engine cost (USD) with a maximum power of P_{ice}^{max}; 424 (USD) represents the baseline coefficient of standard engine cost; C_{cell} stands for the battery cell cost while the count of all battery cells is Num_{bc}.

To ensure the safety and efficiency of battery modular, the third objective is the ISE of battery cells' mean and ambient temperatures. Since large errors will be penalized by ISE, the control system designed to minimize the ISE of battery cells' mean and ambient temperatures would tendency to remove large exceedances above safety thresholds rapidly but also endure small oscillations persevering for a long period.

$$J_3 = \int_0^{t_{end}} \left(T_{avg}(t) - T_{amb}\right)^2 dt \quad (13)$$

where, T_{amb} and T_{avg} are battery cells' ambient temperature and average temperature, respectively. In this context, the multi-objective design issue of HPS can be described as:

$$[\theta_{size}^* \quad \theta_{ems}^*] = \arg\min(J_1 \quad J_2 \quad J_3) \quad (14)$$

in which

$$\left.\begin{array}{l} \theta_{size}^* = [L_{ice}^* \quad \text{Num}_{bc}^*] \\ \theta_{ems}^* = [\phi_{1,\alpha}^* \quad \phi_{1,\beta}^* \quad \phi_{2,\alpha}^* \quad \phi_{2,\beta}^* \quad \phi_{mode}^*] \end{array}\right\} \quad (15)$$

where, θ_{size}^* and θ_{ems}^* are vectors of component sizing parameters and split power control parameters, respectively. To confirm the convergence speed, the input variable needs to be normalized first. The following constraints also need to be satisfied in the optimization process:

$$s.t. \begin{cases} SoC \in [0.2,0.8] \\ n_{mot} \in [0,n_{mot}^+] \\ \tau_{mot} \in [\tau_{mot}^-, \tau_{mot}^+] \\ P_{ice} \in [0, P_{ice}^+] \\ P_{gen} \in [0, P_{gen}^+] \end{cases} \quad (16)$$

where battery SoC needs to be confined within the range [0.2,0.8] for the safe and efficient utilization; n_{mot}^+ reflects the traction motor's maximum speed; T_{mot}^- and T_{mot}^+ stand for the traction motor's minimum and maximum torques, respectively. P_{ice}^+ and P_{gen}^+ represent the ICE's and ISG's maximum powers, respectively. All power sources need to be operated within their permittable ranges.

IV. Electrothermally-Aware Multi-objective Modular Design

In this study, the electrothermal dynamics-conscious multi-objective module design is driven by PACO framework with three multi-objective evolutionary algorithms (MOEAs).

A. Pareto-Augmented Collaborative Optimization

In theory, combining optimization algorithms especially the ones with significantly different computation mechanisms is capable of improving the resultant Pareto frontier [21]. In this paper, three multi-objective evolutionary algorithms (MOEAs) are integrated within a PACO framework to expand the Pareto frontier's distribution. These MOEAs are the elitist non-dominated sorting genetic algorithm (NSGA-II), improved

strength Pareto evolutionary algorithm (SPEA-II), and MOEA based on decomposition (MOEA/D). With help of the PACO framework, the approximated PF could be found through arranging three PFs obtained via NSGA-II, SPEA-II, and MOEA/D, separately.

B. Desirability Function Approach

For the determination of modular specification and control parameters, the desirability function is applied to extract the optimal compromise solution based on the Pareto frontier. From the work of Pasandideh et al., an approach is introduced to calculate a penalty score α for each objective vector in a collection of estimated PFs. Within this context, the solution with a min α becomes the best compromised one. Here the desirability function can be described as:

$$\min_{K \in PF} \alpha\big(J(K)\big) = \min_{K \in PF} \sum_{i=1}^{3} w_i \frac{J_i(K) - J_i^{\min}}{J_i^{\max} - J_i^{\min}} \quad (17)$$

$$\begin{cases} J = [J_1 \quad J_2 \quad J_3] \\ K = [\boldsymbol{\theta}_{size}^* \quad \boldsymbol{\theta}_{ems}^*] \\ \sum_{i=1}^{3} w_i = 1 \text{ and } w_i \geq 0 \end{cases} \quad (18)$$

where $J_i^{\max}$ and $J_i^{\min}$ represent the max and min values of J_i on the approximated PF, respectively. K and w_i stand for the variable vector and weight factor, respectively.

V. RESULTS AND DISCUSSION

In this study, two genuine WLTCs replicated by two human drivers on an undercarriage dynamometer from China Automotive Technology & Research Center are adopted for evaluating the proposed method. Here the comparison of acceleration-velocity distributions between the original (Cycle A) and other replicated cycles (Cycle B and Cycle C) are displayed in Fig. 2. Within both the medium and fast range (70-130km/h), the acceleration of replication cycles becomes further offensive, particular for cycle C.
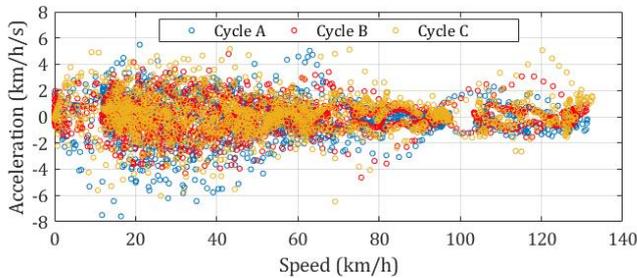
Fig. 2. Velocity-acceleration distribution of realistic WLTCs

A. Multi-objective Optimization Performance

Fig. 3(a) shows the approximate PFs using PACO that integrates NSGA-II, SPEA-II, and MOEA/D, where an estimated PF is captured from the non-dominated group of all approximate PFs. According to the desirability function method with weight factors $w = [0.4 \ 0.4 \ 0.2]$, a needed method (a light blue circle represented) can be obtained. To ensure the fairness of comparison, all algorithms for the optimization are set with the same species size $N = 20, 50, 100$, same record scale, i.e., $\overline{N} = 50$, same probability

of the cruciate and variation ratios, i.e., $p_{cro} = 0.7$ and $p_{mut} = 0.3$, as well as same ending criteria with less than 100 iterations.
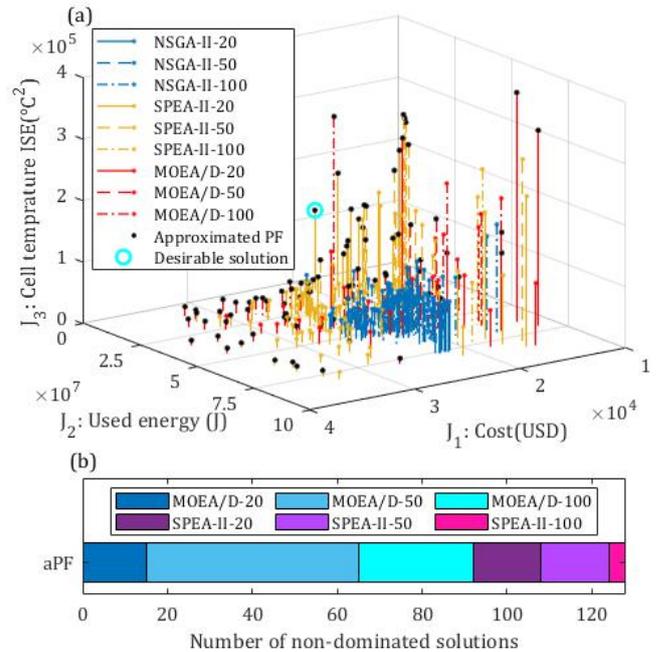
Fig. 3. Pareto frontier comparison based on different evolutionary optimization algorithms: a) expected Pareto frontiers; and b) range of count of non-dominated solutions.

According to the scatter plot, the approximate PFs from NSGA-II (blue points) has the smaller propagates and distribution in comparison with those received from SPEA-II and MOEA/D. As shown in Fig. 3(b), more non-dominated solutions can be collected by PACO, which presents at least 28% increase in comparison with the individual algorithms. Besides, 72% non-dominated solutions are obtained by MOEA/D, while the remaining 28% are produced by SPEA-II. However, NSGA-II does not produce any non-dominated solutions in this experiment. Among different population sizes, a population with 50 individuals could generate around 66% dominion in the estimated PF, while the population size of 20 and 100 generates 23% and 31% dominions, respectively.

TABLE I
OPTIMIZATION PERFORMANCE COMPARISON OVER THREE EVOLUTIONARY ALGORITHMS

Population	Optimization algorithm	GD		HV	
		Mean	SD	Mean	SD
20	NSGA-II	3.42e+7	9.91e+14	2.00e-3	3.27e-6
	SPEA-II	5.88e+6	2.98e+13	2.36e-1	4.87e-2
	MOEA/D	1.02e+6	9.40e+11	3.11e-1	8.56e-2
50	NSGA-II	1.28e+7	1.43e+14	1.30e-2	1.46e-6
	SPEA-II	1.82e+6	3.07e+12	2.62e-1	6.18e-2
	MOEA/D	1.77e+6	2.82e+12	3.08e-1	8.67e-2
100	NSGA-II	4.63e+6	1.97e+13	6.10e-2	3.30e-3
	SPEA-II	3.47e+6	1.14e+13	2.82e-1	1.06e-1
	MOEA/D	1.63e+6	2.51e+12	3.34e-1	7.51e-2

In order to quantify the converge and expected PF group distribution of the methods mentioned above, two widely-applied indicators including the generational distance (GD)

Testing cycle	Optimization algorithm	Cost functions weighted value			Cost of the ICE and battery cells (10^4 USD)			Energy consumption (10^7J)			ISE of battery cell temperature ($10^{4o}C^2$)		
		15°C	25°C	35°C	15°C	25°C	35°C	15°C	25°C	35°C	15°C	25°C	35°C
Cycle A	NSGA-II	0.614	0.687	0.602	2.021	2.403	2.329	3.234	2.499	2.930	17.27	1.668	0.496
	SPEA-II	0.496	0.646	0.507	1.616	2.361	2.223	2.656	2.288	1.795	4.675	1.081	0.625
	MOEA/D	**0.434**	**0.604**	**0.506**	1.600	2.354	1.768	1.776	1.900	2.860	15.79	0.971	1.378
Cycle B	NSGA-II	0.654	0.692	0.648	2.021	2.403	2.329	3.835	2.692	3.627	11.27	0.969	0.357
	SPEA-II	0.538	0.692	0.551	1.616	2.361	2.223	3.288	2.756	3.504	3.505	1.027	1.600
	MOEA/D	**0.483**	**0.688**	**0.539**	1.600	2.354	1.768	2.510	2.703	2.285	24.47	1.141	0.417
Cycle C	NSGA-II	1	0.983	0.818	2.021	2.403	2.329	6.037	3.884	5.909	69.77	9.449	2.784
	SPEA-II	**0.518**	0.906	0.898	1.616	2.361	2.223	2.960	3.970	5.827	54.99	5.350	30.677
	MOEA/D	0.563	**0.791**	**0.601**	1.600	2.354	1.768	3.722	3.501	3.164	31.77	1.805	0.832

Note: 15°C, 25°C, 35°C mean the ambient temperature, T_{amb}. All optimized parameters are captured by a weight factor $w = [0.4\ 0.4\ 0.2]$ under Cycle A.

[22] and hypervolume (HV) [23] are used, as summarized in Table I. In comparison with NSGA-II and SPEA-II, MOEA/D with better converge and better PF group distribution produces the lower average value of GD and the higher average value of HV for different species scale. According to Fig. 3(a), there are orders of magnitude gap of NSGA-II's performance in terms of the average value of HV from the other two. In comparison with NSGA-II and SPEA-II, MOEA/D achieved at least 2.7% reduction in the generational distance and at least 17.6% increase in hypervolume. Therefore, it is evident that MOEA/D is a satisfactory solver for this complicated nonlinear optimization problem.

B. Vehicle System Performance and Robustness

Driver behavior is an essential factor which affects the fuel economy [24,25]. The robustness of the vehicle system enhanced by PACO is examined in this subsection. Each case is repeatedly run under the standard Worldwide Harmonized Light Vehicle Test Cycle (WLTC) for two rounds with an original SoC of 0.8. Then the optimized outcome is adopted in the HPS for various driving scenes such as Cycle A to Cycle C.

Table II shows the performance of the vehicle system as four parts: 1) cost functions weighted value; 2) cost of the ICE and battery cells; 3) sum consumption of energy; and 4) ISE of battery cell temperature. Three ambient temperature levels including 15°C, 25°C, 35°C are investigated. For the HPS robustness measurements against Cycle B and Cycle C, using the parameters improved by MOEA/D produces a cost function value reduced by 31.0%. That is significantly lower than that using the parameters optimized by NSGA-II (62.9%) and SPEA-II (77.1%). In conjunction with Fig. 2, as the driving becomes more offensive (such as Cycle A to Cycle C), the vehicle allocation deduced from MOEA/D is able to better curb the growth of the sum consumption of energy. In comparison with this consumption growth deduced from NSGA-II (able to 101.7%) and SPEA-II (able to 224.7%), while MOEA/D can limit the growth within 10.6%. It is worth noting that for the offensive Cycle C, the vehicle system designed by MOEA/D keep being capable of regulating cell temperature ISE efficiently under different ambient temperature conditions, while other two methods are difficult to curb the energy consumption.
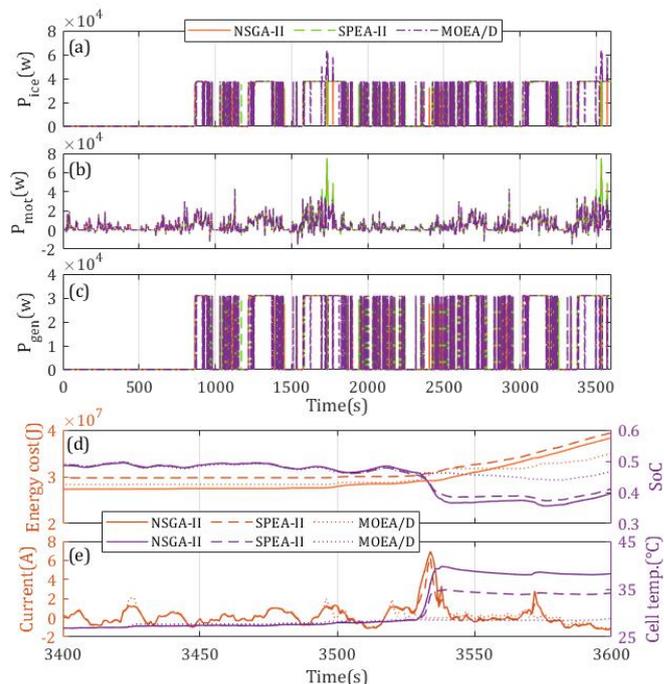
Fig. 4. Real time performance under Cycle C with ambient temperature, $T_{amb} = 25°C$

For further exploration of the underlying reasons to this, the illustrative variables of the vehicle system dependent on time over Cycle C at $T_{amb} = 25°C$ illustrated in Fig. 4. It is evident that the energy-flow trends of HPSs improved by NSGA-II, SPEA-II, and MOEA/D become similar in the hybrid mode. The exhaustive instantaneous performance in one of the peak power requirements $t \in [3400,3600]$ are shown in Figs. 7(d)-(e), while the detected overshooting of the battery cell current within the HPS optimized by SPEA-II could lead to two hidden issues. The first is that the continuous battery high temperature could speed up aging and diminish the charge or discharge efficiency. The second one is that the low SoC could cause the reduction of the allocation's flexibility related to energy flow hence further decreases the entire hybrid system's efficiency. Obviously, HPS optimized by MOEA/D ($T_{avg}^{max} = 28.8°C, SoC_{end} = 0.46$) is capable of better addressing these

issues than NSGA-II ($T_{avg}^{max} = 34.8°C, SoC_{end} = 0.41$) and SPEA-II ($T_{avg}^{max} = 40.0°C, SoC_{end} = 0.40$).

VI. CONCLUSIONS

This paper has proposed an optimized modular design method considering the battery electrothermal dynamics for a Sequence-Parallel HPSs. Using a state-of-the-art electrothermal battery model and a derived sub-objective related to temperature, both battery thermoelectricity dynamics in the design of HPS module can be considered simultaneously. Through extensive numerical simulations with lab made WLTCs for validation purpose, the performance of the introduced method is assessed according to multi-objective optimization, vehicle system robustness, and modular adaptation for various cases. Several conclusions can be summarized as:

1) In the HPS modular design, PACO framework can produce more non-dominated solutions, further leading to at least 28% increase of non-dominated solutions in comparison with individual algorithms.

2) In the PACO, MOEA/D plays a key role in achieving at least 2.7% reduction in generational distance and at least 17.6% increase in the hypervolume, in comparison with NSGA-II and SPEA-II.

3) In the robustness experiments based on Cycle B and Cycle C, the HPS adopting the parameters obtained from MOEA/D is able to produce the cost function value within only 31.0% increase, which is much lower than those adopt parameters from NSGA-II (62.9%) and SPEA-II (77.1%).

References

[1] S. M. Shiva Nagendra, U. Schlink, V. Dheeraj Alshetty, M. Diya, and J. S. Menon, *Traffic-related air pollution, human exposure, and commercially available market solutions: Perspectives from the developing nation context*, no. iii. Elsevier Inc., 2020.

[2] J. Li *et al.*, "Pedestrian-Aware Supervisory Control System Interactive Optimization of Connected Hybrid Electric Vehicles via Fuzzy Adaptive Cost Map and Bees Algorithm," *IEEE Trans. Transp. Electrif.*, vol. 7782, no. c, pp. 1–1, 2021, doi: 10.1109/tte.2021.3124606.

[3] J. Li, Q. Zhou, Y. He, H. Williams, H. Xu, and G. Lu, "Distributed Cooperative Energy Management System of Connected Hybrid Electric Vehicles with Personalized Non-Stationary Inference," *IEEE Trans. Transp. Electrif.*, vol. 7782, no. c, pp. 1–1, 2021, doi: 10.1109/tte.2021.3127142.

[4] J. Li, Q. Zhou, H. Williams, and H. Xu, "Back-to-back competitive learning mechanism for fuzzy logic based supervisory control system of hybrid electric vehicles," *IEEE Trans. Ind. Electron.*, vol. 67, no. 10, pp. 8900–8909, 2020, doi: 10.1109/TIE.2019.2946571.

[5] Q. Zhou *et al.*, "Modified Particle Swarm Optimization with Chaotic Attraction Strategy for Modular Design of Hybrid Powertrains," *IEEE Trans. Transp. Electrif.*, 2020, doi: 10.1109/TTE.2020.3014688.

[6] K. Liu, K. Li, Q. Peng, and C. Zhang, "A brief review on key technologies in the battery management system of electric vehicles," *Front. Mech. Eng.*, vol. 14, no. 1, pp. 47–64, 2019, doi: 10.1007/s11465-018-0516-8.

[7] C. Zhang, K. Li, S. Mcloone and Z. Yang, "Battery modelling methods for electric vehicles - A review," 2014 European Control Conference (ECC), 2014, pp. 2673-2678.

[8] X. Hu, S. Li, and H. Peng, "A comparative study of equivalent circuit models for Li-ion batteries," *J. Power Sources*, vol. 198, no. November 2017, pp. 359–367, 2012, doi: 10.1016/j.jpowsour.2011.10.013.

[9] R. Xiong, J. Tian, W. Shen, and F. Sun, "A Novel Fractional Order Model for State of Charge Estimation in Lithium Ion Batteries," *IEEE Trans. Veh. Technol.*, vol. 68, no. 5, pp. 4130–4139, 2019, doi: 10.1109/TVT.2018.2880085.

[10] Y. Xie *et al.*, "An improved resistance-based thermal model for prismatic lithium-ion battery charging," *Appl. Therm. Eng.*, vol. 180, no. July, p. 115794, 2020, doi: 10.1016/j.applthermaleng.2020.115794.

[11] C. Zhang, K. Li, J. Deng and S. Song, "Improved Realtime State-of-Charge Estimation of LiFePO4 Battery Based on a Novel Thermoelectric Model," in IEEE Transactions on Industrial Electronics, vol. 64, no. 1, pp. 654-663, Jan. 2017.

[12] C. Zhang, K. Li, J. Deng and S. Song, "Improved Realtime State-of-Charge Estimation of LiFePO4 Battery Based on a Novel Thermoelectric Model," in IEEE Transactions on Industrial Electronics, vol. 64, no. 1, pp. 654-663, Jan. 2017.

[13] X. Hu, F. Feng, K. Liu, L. Zhang, J. Xie, and B. Liu, "State estimation for advanced battery management: Key challenges and future trends," *Renew. Sustain. Energy Rev.*, vol. 114, no. August, p. 109334, 2019, doi: 10.1016/j.rser.2019.109334.

[14] K. Liu, X. Hu, Z. Yang, Y. Xie, and S. Feng, "Lithium-ion battery charging management considering economic costs of electrical energy loss and battery degradation," *Energy Convers. Manag.*, vol. 195, no. February, pp. 167–179, 2019, doi: 10.1016/j.enconman.2019.04.065.

[15] M. Ehsani, Y. Gao, S. Longo, and K. Ebrahimi, *Modern electric, hybrid electric, and fuel cell vehicles*. CRC press, 2018.

[16] A. Brooker *et al.*, "ADVISOR Advanced Vehicle Simulator," *National Renewable Energy Laboratory*, 2013. http://adv-vehicle-sim.sourceforge.net/.

[17] Guzzella, Lino and C. Onder, *Introduction to modeling and control of internal combustion engine systems*. Springer Science & Business Media, 2009.

[18] X. Lin *et al.*, "A lumped-parameter electro-thermal model for cylindrical batteries," *J. Power Sources*, vol. 257, no. July, pp. 12–20, 2014, doi: 10.1016/j.jpowsour.2014.01.097.

[19] C. Park and A. K. Jaura, "Dynamic Thermal Model of Li-Ion Battery for Predictive Behavior in Hybrid and Fuel Cell Vehicles," *SAE Tech. Pap.*, vol. 01, no. 2286, 2003, doi: 10.4271/2003-01-2286.

[20] J. Li, Q. Zhou, H. Williams, H. Xu, and C. Du, "Cyber-Physical Data Fusion in Surrogate-assisted Strength Pareto Evolutionary Algorithm for PHEV Energy Management Optimization," *IEEE Trans. Ind. Informatics*, 2021.

[21] J. Zhou and X. Yao, "A hybrid approach combining modified artificial bee colony and cuckoo search algorithms for multi-objective cloud manufacturing service composition," *Int. J. Prod. Res.*, vol. 55, no. 16, pp. 4765–4784, 2017, doi: 10.1080/00207543.2017.1292064.

[22] K. Deb and J. Wiley, *Multi-objective optimization using evolutionary algorithms*. John Wiley & Sons, 2001.

[23] A. Auger, J. Bader, D. Brockhoff, and E. Zitzler, "Theory of the hypervolume indicator：Optimal μ-Distributions and the Choice of the Reference Point," in *Proceedings of the tenth ACM SIGEVO workshop on Foundations of genetic algorithms*, 2009, pp. 87–102, doi: 10.1145/1527125.1527138.

[24] J. Li, Q. Zhou, Y. He, H. Williams, and H. Xu, "Driver-identified Supervisory Control System of Hybrid Electric Vehicles based on Spectrum-guided Fuzzy Feature Extraction," *IEEE Trans. Fuzzy Syst.*, vol. 6706, no. c, pp. 1–1, 2020, doi: 10.1109/tfuzz.2020.2972843.

[25] J. Li et al. "Dual-loop online intelligent programming for driver-oriented predict energy management of plug-in hybrid electric vehicles." Applied Energy 253 (2019): 113617.